CHARACTERISATION OF OXIDE SCALE LAYERS ON IRON-BASED STEELS ON THE NANOSCALE FOR HOT FORGING

[1]Bernd-Arno BEHRENS, [1]Johanna UHE, [2]Thomas LAMPKE, [2]Tim BERGELT, [2]Marcel GRAF, [1]Hendrik WESTER, [1]Simon PEDDINGHAUS, [1]Norman MOHNFELD

[1]Institute of Forming Technology and Machines, Leibniz University Hannover, Garbsen, Germany, EU, behrens@ifum.uni-hannover.de, uhe@ifum-.uni-hannover.de, wester@ifum.uni-hannover.de, s.peddinghaus@ifum.uni-hannover.de, mohnfeld@ifum.uni-hannover.de

[2]Materials and Surface Engineering Group, Institute of Materials Science and Engineering, Chemnitz University of Technology, Chemnitz, Germany, EU, thomas.lampke@mb.tu-chemnitz.de, tim.bergelt@mb.tu-chemnitz.de, macel.graf@mb.tu-chemnitz.de

https://doi.org/10.37904/metal.2024.4893

Abstract

During hot forming, the formation of oxide layers when heating ferrous materials such as steels can hardly be prevented. On the one hand, the formation of oxides is beneficial, as certain oxide phases can have a lubricating effect. On the other hand, oxide scale leads to a loss of material and the hard and brittle phases lead to forging defects and die wear. In the numerical simulation of hot forging processes, the formation of oxide scale layers on workpieces is currently not considered, as there is no suitable numerical approach to address the scale problem and the material-specific characteristic values are missing. In order to describe the behaviour of oxide scale in finite-element simulations, realistic material data is required. In this work, the basis for the characterisation of oxides shall be established. For this purpose, steel specimens of C45 and C60 were oxidized under controlled conditions at elevated temperatures. Subsequently, the specimens were examined through a scanning electron microscope (SEM) and the individual oxide scale layers consisting of wüstite (FeO), magnetite (Fe_3O_4) and hematite (Fe_2O_3) were detected. The specimens were examined using a triboindenter to record the mechanical properties such as nanohardness and modulus of elasticity of each oxide scale component on the nanoscale. XPM (X property mapping) nanohardness mappings were used to visualise the phase transitions and porosity of the oxide scale and compared with the microscopy and SEM images. In addition, magnetite spots in the wüstite oxide layer could be detected through XPM hardness mapping and SEM examinations.

Keywords: Oxide scale layers, C45, C60, Nanoindentation, Scanning electron microscope

1. INTRODUCTION

Hot forming is usually applied to manufacture high-strength mechanical components. Due to the high forming temperatures of over 900 °C, high degrees of deformation can be achieved with comparatively low process forces. With iron-based materials, however, the heating of the semi-finished products leads to the formation of iron oxides. In detail, a three-layered structure can be observed in the oxide layer/scale. Wüstite (FeO) forms the innermost layer and is the interface between the substrate and the oxide skin. Magnetite (Fe_3O_4) is the intermediate layer and hematite (Fe_2O_3) forms the outer layer [1]. Che et al. and Day et al. describe that the formation of oxide scale is mainly dependent on the oxidation temperature, oxidation time, alloy configuration and the atmosphere [2,3]. Similar findings were shown by Wielgosz et al. and Cheng et al., whereby the time and temperature were determined as the dominant influences on the growth rate of oxide scale [4,5]. The increased diffusion processes due to raised temperatures and longer durations lead to an expansion of the layer thickness. Depending on the process conditions, such as oxidation time and temperature, layer

thicknesses of up to 2,000 µm are formed [6]. In addition, Graf et al. described a decreasing scale thickness with increasing carbon content in steels [7]. As a result of oxide scale, the surface properties, friction behaviour and flow properties of the workpiece change compared to an unscaled billet. In addition, oxide scale can lead to increased tool wear and a mass loss of the workpiece of up to 3 %, thereby unnecessarily wasting resources [8]. It was also found that an oxide skin can have a protective character for the workpiece. However, the oxide skin can only provide this protection, if it's free of defects such as cracks or spallation zones [9]. The process design and material development of hot forming processes is carried out mostly numerically, which saves important resources such as material, time and energy. In order to increase the accuracy of these calculations, it is essential to use realistic material data in accordance to the process of interest (e.g. temperature, strain rate, stress state). For this purpose, analytical or semi-analytical material laws in combination with finite element method (FEM)-based simulation are advantageous, as the computation speed is not limited compared to physical material models. In addition to the oxidation behaviour, Graf et al. were able to mathematically describe the flow behaviour of the scale layer in order to use the data in a numerical simulation [7]. The FEM model of the oxide scale was built layer by layer as it was previously assumed that the formation and growth of oxide scale occurs in such a way. However, current investigations show that additional globular inclusions of the other oxide scale layers are also present in the wüstite, which influence the failure behaviour of the oxide scale layer. Clear detection of these inclusions is only possible with great effort using a focussed ion beam (FIB) lamella. The measurement in backscattering mode in the scanning electron microscope (SEM) does not lead to a clear detection due to the reaction of the surrounding material. The aim of this work is to enable determining globular inclusions in oxide scale layers by a combination of SEM analyses and nanoindentation without requiring elaborate and expensive FIB lamellae. In addition to the unambiguous determination of the inclusions, the mechanical properties such as nanohardness and E-modulus of the phase can also be determined and thus material models of the scale layers for FE simulations can be extended.

2. MATERIAL AND METHOD

To analyse the oxide scale layers, cylinders with a diameter of Ø 10 mm and a length of 10 mm were first produced from C45 and 60 by machining. The specimens were then oxidised under controlled conditions. For this purpose, the specimens were placed on an inductive heat source and held at 1,050 °C for 120 s. Heating was carried out at a heating rate of 10 K/s, while cooling was performed at a cooling rate of 5 K/s to minimise spalling of the oxide scale layer. Both specimens, the C45 and C60 were each embedded and then ground along the longitudinal axis of the cylinder to the centre and polished to 0.5 µm and afterwards sputtered with carbon. Using LEO1455VP SEM with EDAX Genesis from Zeiss, the resulting oxide scale layers and the two steels were analysed in backscattered electron (BSE) mode. The layer structure was analysed using BSE and pores, cracks or inclusions were visualised. Energy dispersive X-ray (EDX) spectroscopy was used to analyse the oxide scale layers by means of point and area measurements in order to determine the chemical composition of the resulting oxide scale layers. The mechanical characteristics of the individual oxide scale layers were recorded using nanoindentation with a Hysitron TI 950 triboindenter. A high-precision 3-axis tandem tube piezo scanner, on which a capacitive three-plate transducer (2D transducer) is mounted, was used for the measurements. The three-sided Berkovich diamond tip with a tip radius of less than 50 nm is fixed to the transducer. The Berkovich tip was calibrated on a quartz glass sample in the range from 100 µN to 10,000 µN. An area function was determined which requires a minimum indentation depth of 50 nm according to the method of Oliver and Pharr [10]. The continuous force indentation test was carried out using a trapezoidal force-time function. Due to the continuously measured loading and unloading phase, it is possible to determine not only the nanohardness but also the reduced modulus of elasticity [11]. A normal force of 1,800 µN was selected for the indentation test, as the minimum indentation depth of 25 nm could be exceeded during test measurements in the scale layer. In order to achieve the highest possible resolution in the measurements, an indent was placed every 1.5 µm in a measuring field of 120 µm x 120 µm. This allows individual grains to be

tested separately in the microstructure or inclusions in the scale layer without influencing each other. The measuring point was recorded before and after the measurement using the light microscope optics of the triboindenter. All measurements were carried out under laboratory conditions at constant ambient temperature and humidity.

Large-scale and high-resolution nanohardness maps usually combine several materials or phases with characteristic mechanical properties. These components can be clustered so individual phases are represented in the mapping based on the determined mechanical properties. The maps often consist of large and irregularly shaped data sets for which automatic clustering is useful. For this, the K-Means clustering technique was used to cluster the data, as it works robustly with a large number of data sets. All data is organised into k clusters (C) using the K-Means algorithm based on the Euclidean distance. The number of k is predefined and was set to 4, as in addition to the steel and the embedding material/pores, wüstite and magnetite in particular could be tested with sufficient measuring points. Hematite only occurs as an extremely thin layer in the edge area, and is removed or damaged during the preparation of the specimens, so that clear detection is not possible. When clustering, the hardness and the determined modulus of elasticity are taken into account. This means that only points are included in the respective clusters where both the hardness and the modulus of elasticity lie within the limits determined for the cluster. A specific combination of modulus of elasticity and hardness is characteristic for a particular material or material phase, so that the microstructural distribution is visualised by clustering in the mapping.

3. RESULTS AND DISSCUSION

The oxide scale layers detected in the SEM are shown in (**Figure 1a**) for C60 and in (**Figure 1b**) C45 as a BSE image. For both steel grades, all three oxide scale layers described in the literature could be detected, starting from the steel substrate material, first wüstite, followed by magnetite and a thin layer of hematite. Hematite has already partially been separated from the magnetite layer or was damaged during the specimen preparation, see (**Figure 1a**). The different shades of grey show that the density of the oxide scale layers decreases from wüstite to hematite, as iron is increasingly enriched with oxygen. Although the total layer thickness is smaller for C60 than for C45, only the thickness of the wüstite layer differs. Magnetite and hematite form to the same extent of around 10-12 µm for both investigated steels. In addition to cracks and pores (visible as black areas), the bonding to the steel substrate is also partially damaged. In addition, dark globular inclusions can be seen in the wüstite layer in both specimens, which suggests lighter oxides such as magnetite or hematite. For the EDX measurement, a calibration was first carried out on an hematite standard. EDX spot measurements show Fe contents of 44.81 to 45.74 at.% and O contents from 54.26 to 55.19 at.% for these inclusions, making a clear determination impossible, compare (**Figure 1b**). There are many indications that it is magnetite which has an Fe content of 42.86 at. % and an O content of 57.14 at. %.

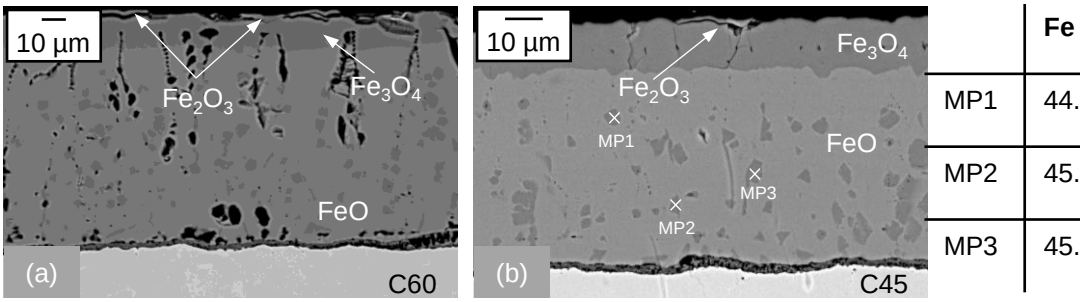

	Fe at %	O at %
MP1	44.81	55.19
MP2	45.06	54.94
MP3	45.74	54.26

Figure 1 BSE images of the oxide scale layer in cross-section of (a) C60, (b) C45 with measuring points (MP1-3) for EDX measurement of the inclusions.

The oxide scale layers were subsequently tested by means of nanoindentation in order to visualise the mechanical properties of the respective phase as a mapping. **Figure 2a** and **2b)** shows the nanohardness

mappings for C60 and C45. Both steels show a similar nanohardness of 4 GPa on average. In the nanohardness mapping, wüstite and magnetite are clearly recognisable within the oxide scale layer and the distribution is also in agreement with the oxide scale from the BSE-images in (**Figure 1a** and **1b)**. Hematite is not clearly recognisable, high nanohardnesses of approx. 13 GPa occur in isolated spots in the edge area. At the same time, a decrease in hardness towards the embedding agent can be observed, which indicates edge rounding due to the specimen preparation. During the indentation of the rounding, the indenter slips due to the one-sided indentation, whereby a greater indentation depth is absorbed and thus the hardness is lower. The hardness values in this area should therefore be regarded as invalid. In addition, pores and cracks can be detected in the mapping through low hardness values. Within the wüstite layer, harder areas repeatedly appear, which correspond to the same hardness level as the magnetite layer of approx. 8 GPa. It is conspicuous that very high hardness values were detected in the transition between the oxide scale layer and the steel, although in the BSE images no bonding could be observed there in some cases. Based on the distribution of the modulus of elasticity, the respective phases can be recognised in the same way as the hardness distribution, but are not as clear through the colour plot, due to the larger range of values. The steel substrates show the highest modulus of elasticity at approx. 205 GPa. Lower moduli of elasticity were measured for the wüstite and magnetite than for the steels.

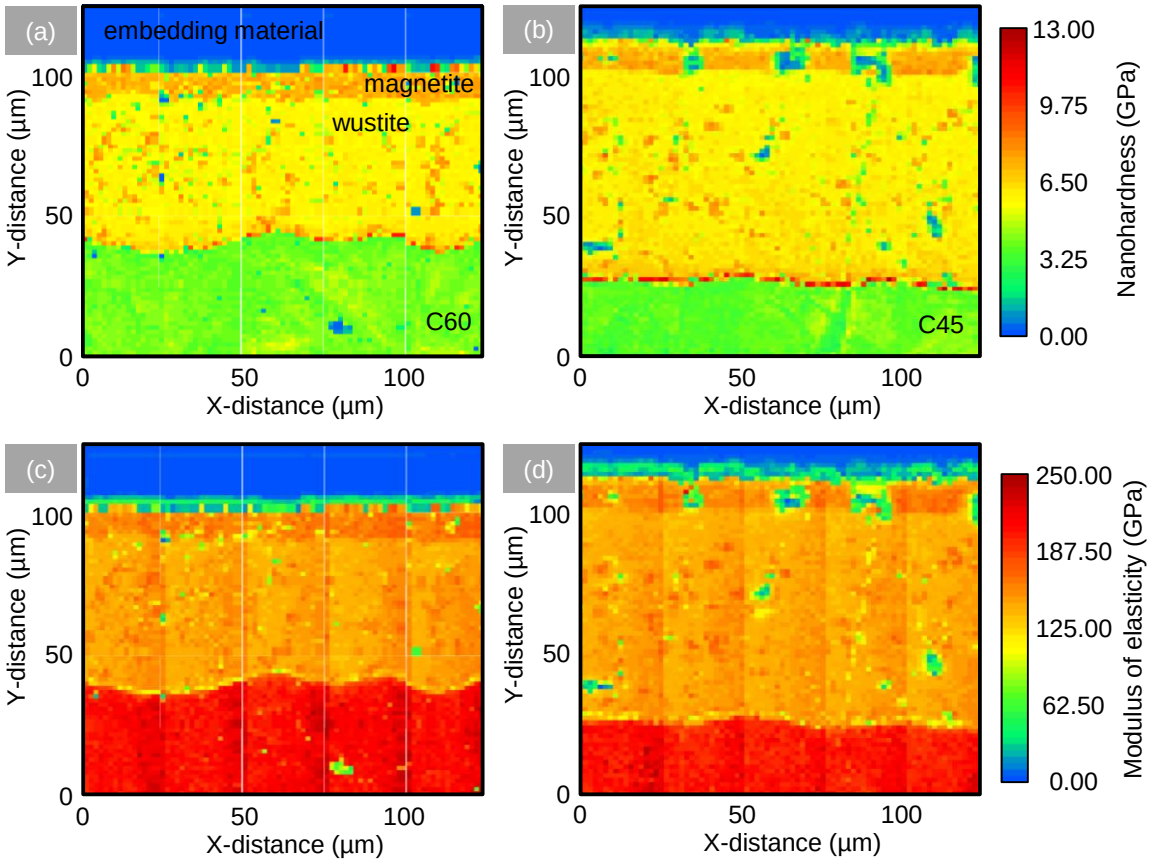

Figure 2 Nanohardness mapping for (a) C60, (b) C45 and modulus of elasticity mapping for (c) C60, (d) C45

The data sets consisting of nanohardness and modulus of elasticity were divided into four clusters using the k-means algorithm. **Table 1** shows the range of the respective clusters in which a pair of values must be located for an assignment to take place and also the average values and the standard deviation for nanohardness and modulus of elastity of the respective cluster. The four clusters were selected on the basis of the BSE images and the hardness mappings.

Table 1 Range of the determined clusters and average values as well as the standard deviation for the nanohardness and the modulus of elasticity

Cluster	Hardness range (GPa)	Modulus range (GPa)	Average hardness (GPa)	Deviation hardness (GPa)	Average modulus (GPa)	Deviation modulus (GPa)
Steel cluster	2.04-5.65	118.98-244.80	3.82	±0.40	202.60	±12.92
Wüstite cluster	2.71-6.87	66.67-186.22	5.92	±0.53	142.54	±9.65
Magnetit cluster	6.69-12.57	126.18-179.77	7.60	±0.93	156.69	±9.02
Embedding cluster	0.19-4.30	3.58-113.04	0.74	±0.75	24.09	±23.24

Clustering results are shown in (**Figure 3a** and **3b)** for C60 and C45. The clusters determined in the mapping show a very good agreement with the distributions of the SEM images and the nanoindentation. In dark blue, the steel was summarised into a cluster. The pairs of values with very low nanohardness and low modulus of elasticity in green describe the embedding material, but also include pores or cracks within the oxide scale layer and the steel, see (**Figure 3a**). The wüstite cluster is shown in red and, analogous to the SEM and hardness mapping investigations, presents the largest area within the oxide scale layer. The position of the magnetite cluster is also shown correctly. In addition to the magnetite layer in the edge area, individual groups of magnetite clusters can be recognised within the wüstite cluster. Comparing the position of the magnetite groups with the light microscope image in (**Figure 3c**), it is evident that the brighter areas correspond to the position of the magnetite groups. Considering the magnetite cluster in the transition to the embedding mass in (**Figure 3b**), it is noticeable that some pairs of values were assigned to the wüstite cluster, although wüstite was not detected in these areas in any examination. Reason for the classification in the wüstite cluster may be the invalid measurement points due to the edge rounding during specimen preparation. The same applies to the isolated points of the steel cluster in (**Figure 3b**) in wüstite but also in magnetite. However, these spots only occur where there was a pore. This means that by indenting the transition from e.g. wüstite to the pore, the indenter slides off and thus a pair of values of nanohardness and modulus of elasticity is created which lies within the steel cluster. The increased hardness values in the transition from wüstite to steel from (**Figure 2b**) were assigned to magnetite custer, see (**Figure 3**).

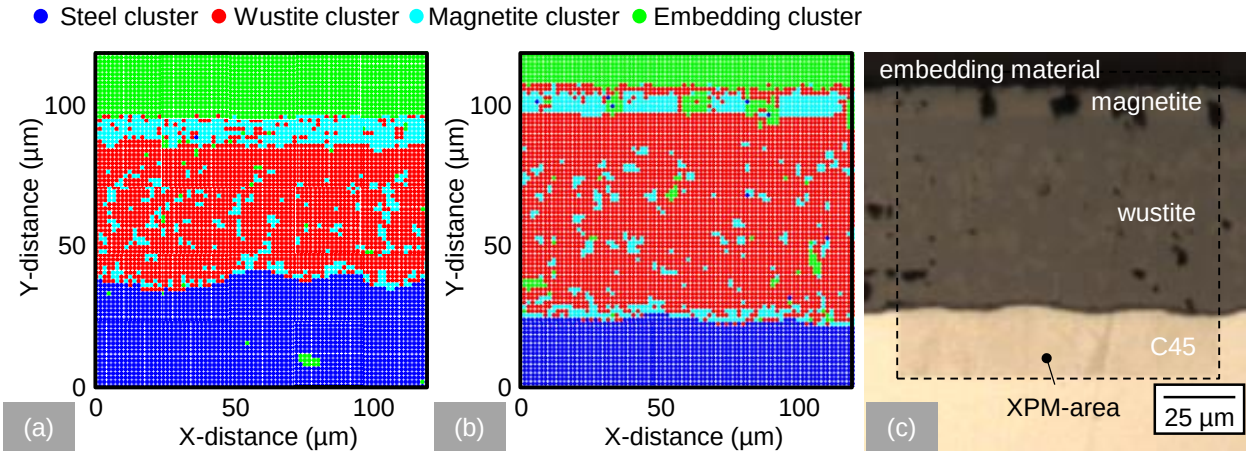

Figure 3 Distribution of the calculated clusters for (a) C60, (b) C45, (c) light microscope image of the measuring location of C45.

4. CONCLUSION

In this work, steel specimens of C60 and C45 were specifically oxidized under controlled conditions and then analysed using SEM and nanoindentation. An oxide scale layer consisting of wüstite (FeO), magnetite (Fe_3O_4)

and hematite (Fe_2O_3) was detected for both steel grades. In addition to the layered structure of the oxide scale layer known from the literature, globular inclusions were also detected within the wüstite layer. Due to the influence of the surrounding material, these could not be clearly identified by EDX. The oxide scale layers were examined with a high resolution of 1.5 µm by nanoindentation. The mappings of hardness and modulus of elasticity showed a good agreement with the layer structure determined in the SEM. By using the k-means algorithm, this data could be divided into four clusters, allowing the distribution of the particular phases to be visualised. The distribution of the clusters also showed a very good agreement with the findings from the SEM, nanoindentation mappings and the optical microscope images of the measurement spot. The globular inclusions within the wüstite layer were assigned to the magnetite cluster, which in combination with the SEM results indicates magnetite islands in the wüstite. By combining SEM, nanoindentation and clustering, it could be shown that it is possible to determine the oxide scale composition near the surface without the need to produce complex FIB lamellae. For the final validation of the method presented here, a FIB lamella should be produced to clearly characterise the magnetite islands. Furthermore, it makes sense to further improve the results of the algorithm by using more clusters. For example, additional areas such as edge rounding can be recognised or the transition area from wüstite to steel can be represented as a separate cluster.

ACKNOWLEDGEMENTS

Funded by the Deutsche Forschungsgemeinschaft (DFG, German Research Foundation) – project number 316273316.

REFERENCES

[1] DAVIES, M. H., SIMNAD, M. T., BIRCHENALL, C. E. On the Mechanism and Kinetics of the Scaling of Iron. *Journal of Metals*. 1951, vol. 3, pp. 889–896.

[2] CHEN, R. Y., YUEN, W. Y. D. Review of the High-Temperature Oxidation of Iron and Carbon Steels in Air or Oxygen, *Oxidation of Metals*. 2002, vol. 59, pp. 433-468.

[3] DAY, M. J., SMITH, G. V. Iron Alloy Scaling, *Industrial and Engineering Chemistry*. 1943, vol. 35, pp. 1098-1103.

[4] WIELGOSZ, E., KARGUL, T., FALKUS, J. Comparison of experimental and numerically calculated thermal properties of steels, In: *Proceedings 23rd International Conference on Metallurgy and Materials*. Brno: METAL, 2014, pp. 1528-1533.

[5] CHENG, X., JIANG, Z., WEI, D., HAO, L., ZHAO, J., JIANG, L. Oxide scale characterization of ferritic stainless steel and its deformation and friction in hot rolling, *Tribology International*. 2015, vol. 84, pp. 61-70.

[6] HUITRON, R.M.P., LÓPEZ, P.E.R., VUORINEN, E., JALALI, P.N., PELCASTRE, L., KÄRKKÄINEN, M. Scale Formation on HSLA Steel during Continuous Casting Part I: The Effect of Temperature–Time on Oxidation Kinetics, *Metals*. 2020, vol. 10, pp. 1243.

[7] GRAF, M., ULLMANN, M., KORPALA, G., WESTER, H., AWISZUS, B., KAWALLA, R., BEHRENS, B.-A. Forming and Oxidation Behavior During Forging with Consideration of Carbon Content of Steel, *Metals*. 2018, vol. 8, pp. 996.

[8] LUONG, L., HEIJKOOP, T. THE INFLUENCE OF SCALE ON FRICTION IN HOT METAL WORKING, *Wear*. 1981, vol. 71, pp. 93-102.

[9] SCHÜTZE, M. Mechanical properties of oxide scales, *Oxid Met*. 1995, vol. 44, pp. 29–61.

[10] OLIVER, W.C., PHARR, G.M. An improved technique for determining hardness and elastic modulus using load and displacement sensing indentation experiments, Journal of materials research, 1992, vol. 7, pp. 1564–1583.

[11] FISCHER-CRIPPS, A.C. Nanoindentation. New York: Springer Science + Business Media LLC, 2011.

[12] MURPHY, K. P. Machine Learning: A Probabilistic Perspective. Cambridge: MIT Press, 2012.

[13] ARTHUR, D., VASSILVITSKII, S. k-means++: The advantages of careful seeding, Soda. 2007, vol. 7, pp. 1027-1035.